JOURNAL OF GEOPHYSICAL RESEARCH: SPACE PHYSICS, VOL. 118, 502–514, doi:10.1029/2012JA018146, 2013

Ion gyroharmonic structures in stimulated radiation during second electron gyroharmonic heating: 1. Theory

A. Samimi,[1] W. A. Scales,[1] H. Fu,[1] P. A. Bernhardt,[2] S. J. Briczinski,[2] and M. J. McCarrick[3]

Received 23 July 2012; revised 31 October 2012; accepted 10 November 2012; published 31 January 2013.

[1] Stimulated electromagnetic emissions (SEEs) may provide important diagnostic information about space plasma composition, energetics, and dynamics during active experiments in which ground-based high-powered radio waves are transmitted into the ionosphere. The nonlinear plasma processes producing this secondary radiation are not well understood particularly for some recent observations where the transmitter (pump) frequency is near the second harmonic of the electron gyrofrequency. New, more comprehensive, experimental observations of spectral features within 1 kHz of the pump wave frequency are reported here to begin more careful comparisons of the experimental observations and a possible theoretical underpinning, which is also provided. The experimental observations typically show two distinct types of secondary radiation spectra, which are (a) discrete narrowband harmonic spectral structures ordered by the ion gyrofrequency and (b) broadband spectral structure with center frequency near 500 Hz and similar spectral bandwidth. A theoretical model is provided that interprets these spectral features as resulting from parametric decay instabilities in which the pump field ultimately decays into high-frequency upper hybrid/electron Bernstein and low-frequency neutralized ion Bernstein and/or obliquely propagating ion acoustic waves at the upper hybrid interaction altitude. Detailed calculations of the threshold level, growth rate, unstable wave number, and frequency bandwidth of the instabilities are provided for comparisons with experimental observations. An assessment of the effect of the critical instability parameters are provided including pump electric field strength, proximity of the pump frequency to the electron gyrofrequency and pump electric field geometry. The model shows quite reasonable agreement with the experimental observations. Further discussions are provided of connections with past observed SEE spectral features and potential new diagnostic information provided by these newly categorized spectra.

Citation: Samimi, A., W. A. Scales, H. Fu, P. A. Bernhardt, S. J. Briczinski, and M. J. McCarrick (2013), Ion gyroharmonic structures in stimulated radiation during second electron gyroharmonic heating: 1. Theory, *J. Geophys. Res. Space Physics*, *118*, 502–514, doi:10.1029/2012JA018146.

1. Introduction

[2] Since the experimental discovery of stimulated electromagnetic emissions (SEEs) [*Thidé et al.*, 1982], generated during heating experiments by a powerful HF electromagnetic wave, numerous studies [*Leyser*, 2001] have been conducted to understand its generation process. The SEE spectra contain diagnostic information about the ionosphere. For instance, the SEE spectral features can be employed to determine electron temperatures [*Bernhardt et al.*, 2009] or the amplitude of a local geomagnetic field in the interaction region of the ionosphere [*Leyser et al.*, 1992]. Parametric decay of the pump field into new plasma wave modes has been considered as a fundamental process that may explain the characteristics of the SEE spectral sidebands. The electromagnetic (EM) pump wave can be directly involved in the decay process and generate new EM and electrostatic (ES) waves. For example; the decay of the pump field into ion acoustic (IA) and scattered EM waves is involved in the stimulated Brillouin

[1]The Bradley Department of Electrical and Computer Engineering, Virginia Tech, Blacksburg, Virginia, USA.
[2]Plasma Physics Division, Naval Research Laboratory, Washington, DC, USA.
[3]Marsh Creek, LLC, Gakona, Alaska, USA.

Corresponding author: A. Samimi, The Bradley Department of Electrical and Computer Engineering, Virginia Tech, Whittemore Hall, Blacksburg, VA 24061, USA. (arsamimi@vt.edu)

2169-9380/13/2012JA018146

scatter process [*Norin et al*., 2009]. On the other hand, for other SEE features, the EM wave undergoes conversion to another ES wave, which then decays into new ES waves that are then converted back to EM waves. For instance, parametric decay of an upper hybrid/electron Bernstein (UH/EB) pump wave into another UH/EB wave and lower hybrid (LH) wave [*Zhou et al*., 1994; *Bernhardt et al*., 1994] is proposed for generation of the downshifted maximum feature. The downshifted peak (DP) is considered to be generated through the decay of an electron Bernstein (EB) pump field into another EB and an IA wave [*Huang and Kuo*, 1995]. A thermal oscillating two-stream instability (OTSI) could be responsible for the conversion of the EM wave into an ES upper hybrid (UH) pump wave [*Grach et al*., 1978; *Das and Fejer*, 1979; *Dysthe et al*., 1983; *Huang and Kuo*, 1994]. The conversion process may be followed by an explosive growth through a wave trapping process so-called resonance instability [*Inhester*, 1982; *Dysthe et al*., 1982; *Vaskov and Gurevich*, 1977].

[3] The first observation of the structures ordered by the ion gyrofrequency near 45 to 50 Hz in the SEE spectrum was reported by *Thidé et al*. [1983]. These ion gyroharmonic structures were observed during the extraordinary transmission (X-mode) on 2.759 MHz that is very close to the local second electron gyroharmonic frequency. Parametric decay of the extraordinary EM wave into the UH wave and ion Bernstein (IB) was proposed for the generation mechanism of the aforementioned structures [*Sharma et al*., 1993]. A clearer SEE spectrum containing the ion gyroharmonic structures was observed during the heating in the ordinary (O-mode) transmission on 2.85 MHz [*Bernhardt et al*., 2011]. The spectrum may show up to 16 discrete spectral lines and is distinctly different from magnetized stimulated Brillouin scatter in which only one spectral line near the cyclotron frequency is observed [*Bernhardt et al*., 2009]. Parametric decay of the EM pump wave into EB and IB in the reflection altitude has been proposed as a generation mechanism of the ion gyroharmonic structures [*Bernhardt et al*., 2011]. Neglecting the damping rates and by using an analytical expression, threshold electric field intensity required for this process was estimated to be 250 V/m [*Bernhardt et al*., 2011]. In addition to the ion cyclotron structures, some of the experimental measurements exhibit a broadband spectral feature downshifted from the pump frequency within 1 kHz that has embedded ion gyroharmonic structures. In this paper, new observations of the ion gyroharmonic structures and the broadband feature are presented. Moreover, experimental evidences regarding simultaneous excitation of the ion gyroharmonic structures and the magnetized stimulated Brillouin scatter (MSBS) are also provided. For the first time, temporal evolution of these structures is considered in some detail. Furthermore, experimental data are provided that exhibits ion gyroharmonic structures in the SEE spectrum for heating at low 0.8 MW power corresponding to 63 MW effective radiated power (ERP) at 2.80 MHz.

[4] The object of this paper is to investigate the generation of ion gyroharmonic structures and associated broadband spectral features within 1 kHz of the pump frequency, and to provide fundamental parameters that characterize these types of spectra that may have critical diagnostic information of the heated plasma. The results presented here are for heating at the second electron gyroharmonic. There has been considerable interest in second gyroharmonic heating recently due to creation of artificial ionization layers and potential applications [*Pedersen et al*., 2010, 2011]. The results here are most likely applicable to heating at gyroharmonics for $n > 2$ and this is noted and discussed later.

[5] This paper is organized as follows. In the next section, the experimental procedure is stated. Then experimental observations are provided. Next, an analytical model is used to estimate the pump field strength in the interaction region. Parametric decay instability is then considered. The impact of (1) the pump field strength, (2) its frequency relative to the electron gyroharmonic frequency, and (3) angle of the pump field relative to the geomagnetic field on the SEE spectrum are considered. The threshold of the electric field strength is also calculated and compared to the previous estimation. Finally, summary and conclusions are provided.

2. Experimental Procedure

[6] To obtain the SEE spectra, a 30 m folded dipole antenna and a receiver with around 90 dB dynamic range was set up close to the High Frequency Active Auroral Research Program (HAARP) site (63.09°N, –145.15°E) in Gakona, Alaska. The receiver shifts the frequency of the acquired signal by the heater frequency by mixing, and sampling it at 250 kHz. The acquired in-phase and quadrature-phase (I and Q) data are postprocessed by utilizing Blackman window and then the fast Fourier transform to obtain spectrograms of the received signal. The frequency resolution of the spectrums corresponding to the discrete ion gyroharmonic structures and the broadband spectral features are 0.95 and 3.8 Hz, respectively. The experiments were carried out in O-mode. Three sets of experiments were designed to examine the effect of the heating cycle, the pump field strength and angle of the transmission on the ion gyroharmonic structures. The latter experiment was conducted on 25 July 2011 from 03:48 UT to 04:48 UT during which the ionospheric absorption was too high and no SEE features were observed. In all other experiments the heater beam was pointed to the magnetic zenith with an azimuth of 202° and a zenith angle of 14°. Discrete ion gyroharmonic structures in the SEE spectra were observed during the first two sets of experiments. These experiments were conducted in the nighttime on 21 July from 10:01 UT to 11:01 UT (02:01–03:01 local time). The reflection altitude was roughly around 250 km according to the measurements of the digital ionosonde at HAARP. The geomagnetic field strength above HAARP is estimated to be $B_0 = 50,524.8$ nT using the International Geomagnetic Reference Field (IGRF) model. Correspondingly, the electron gyrofrequency is at $f_{ce} = 1.412$ MHz and ion gyrofrequency is at $f_{ci} = 48.07$ Hz. In the first 6 min of the experiment, the power spectrum of the received signal does not show usable SEE data. Examination of the digital ionosonde measurements shows that the ionosphere was absent from 09:30 UT to around 10:05 UT.

[7] In the first set of experiments the heater duty cycle was increased in 30 s steps starting from 30 s on and 30 s off cycle and continued to 240 s on and 240 s off cycle. The discrete ion gyroharmonic structures appeared in the spectrum of the experiments in which the heater duty cycle was more than 90 s on and 90 s off. Furthermore, the power spectrum

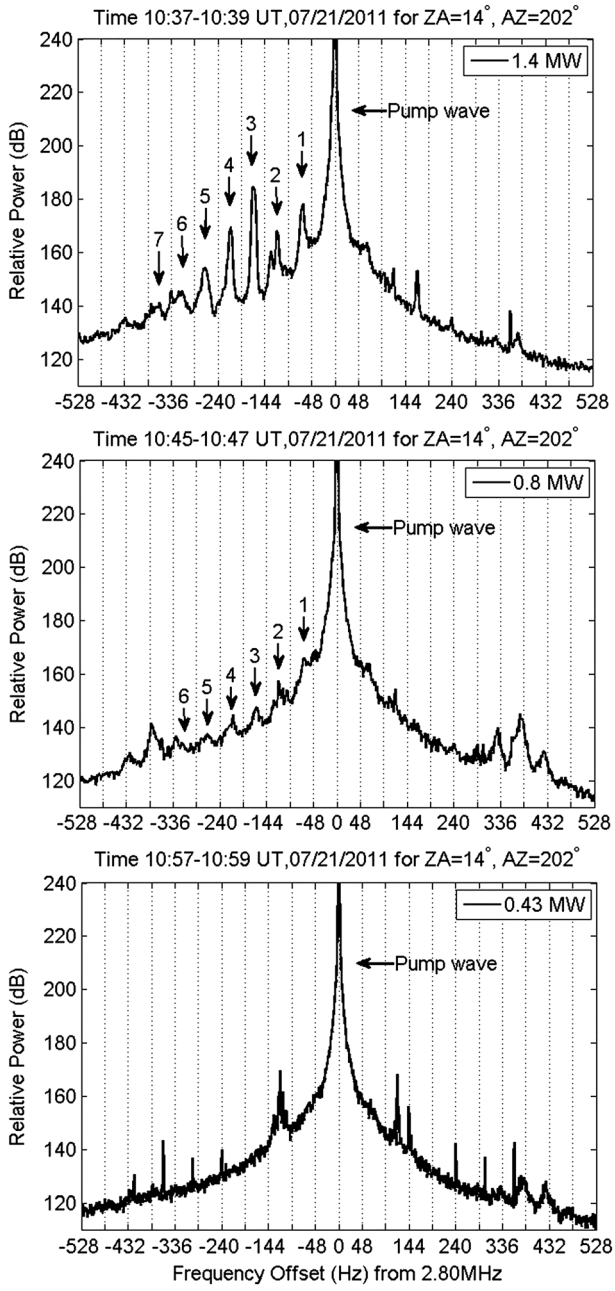

Figure 1. Stimulated electromagnetic emission spectra recorded at HAARP showing ion gyroharmonic structures for $\boldsymbol{P_{heater} = 1.4}$ MW, $\boldsymbol{P_{heater} = 0.8}$ MW, $\boldsymbol{P_{heater} = 0.43}$ MW. Heater duty cycle was 120 s on and 120 s off. The power spectrum in the bottom panel corresponding to $\boldsymbol{P_{heater} = 0.43}$ MW does not show SEE feature indicating heater power is below the threshold level. The heater frequency was tuned to 2.80 MHz, close to the local second electron gyroharmonic frequency. Dotted lines are at the ion gyrofrequency. Note that the ion gyroharmonic structures are downshifted relative to the pump frequency.

of the experiments with longer duty cycles shows sharper discrete structures. Although, this experiment may imply correlation between the generation of the discrete ion gyroharmonic structures and the heater duty cycle, occasionally, the power spectrum of some of the experiments that were carried out on 22 July between 06:00 UT and 07:00 UT for which the heater duty cycle was 30 s on and 60 s off also shows sharper discrete ion gyroharmonic structures. These structures downshifted from the heater frequency correspond to the 6^{th}–13^{th} harmonics of the ion gyrofrequency, respectively. Additionally, as we mentioned before, the ionosphere was absent until around 10:05 UT. On the other hand, the first three experiments for which the heater duty cycle was 30 s on and 30 s off, 60 s on and 60 s off, and 90 s on and 90 s off were conducted from 10:01 UT to 10:07 UT. Thus, correlation between the heating cycle and generation of the ion gyroharmonic structures is still not understood. It is subject to more experimental investigation in the future to reach to the final conclusion. In addition to the aforementioned experiments, the effect of the heater duty cycle on the discrete ion gyrostructure was examined again on 23 July 2011 from 04:36 UT to 04:55 UT. Although during this experiment, the ionosphere was relatively quiet and the critical frequency was around 5 MHz, but no ion gyroharmonic structure was seen in the SEE spectrum. One of the SEE spectra during this experiment shows the broadband spectral feature that will be explained in the next section.

[8] In the second set of experiments heater duty cycle was 120 s on and 120 s off. The heater power was reduced in 1 dB steps to find the threshold level for generation of the ion gyrostructures. The minimum heater power for which the ion gyrostructures formed was $P_{heater} = 0.8$ MW (63 MW ERP). To see ion gyroharmonic structures in the SEE spectrum of the experiments corresponding to low transmitter power such as 1 MW or 0.8 MW, the fast Fourier transform should be taken in between transients produced by the HAARP transmitter at turn on and turn off. Occasionally, during another experiment that was initially designed to study the spectrum of the MSBS, the broadband spectral feature with embedded discrete ion gyroharmonic structure was observed. Further details of this experiment are presented in the next section.

3. Experimental Results

3.1. Discrete Harmonic Spectral Features

[9] Spectra showing the discrete ion gyroharmonic structures were obtained during the experiments conducted on 21 July 2011 from 10:11 UT to 11:01 UT. Figure 1 shows the power spectrum of the acquired signal for $P_{heater} =$ 1.4 MW (111 MW ERP), $P_{heater} = 0.8$ MW (63 MW ERP), and $P_{heater} = 0.4$ MW (31 MW ERP).

[10] The heater duty cycle was 120 s on and 120 s off. The transmitter frequency was tuned near the local second electron gyroharmonic at $f_{heater} = 2.8$ MHz. The ion gyrostructures are weaker at the lower heater power and the threshold is $P_{heater} \cong 0.8$ MW. The observed structures are shifted below the pump frequency by approximately half harmonics of the ion gyrofrequency. This leads us to believe that the structures are produced by a parametric decay process involving neutralized ion Bernstein waves as will be described later. Figure 2 shows the power spectrum taken over 5 s intervals during the heating process in which the heater power was 1.4 MW. This provides the temporal evolution of the spectrum. The corresponding spectrogram is shown in Figure 3. Almost all the ion gyroharmonic structures appear above the noise level of the spectrum approximately 6 s after the heater

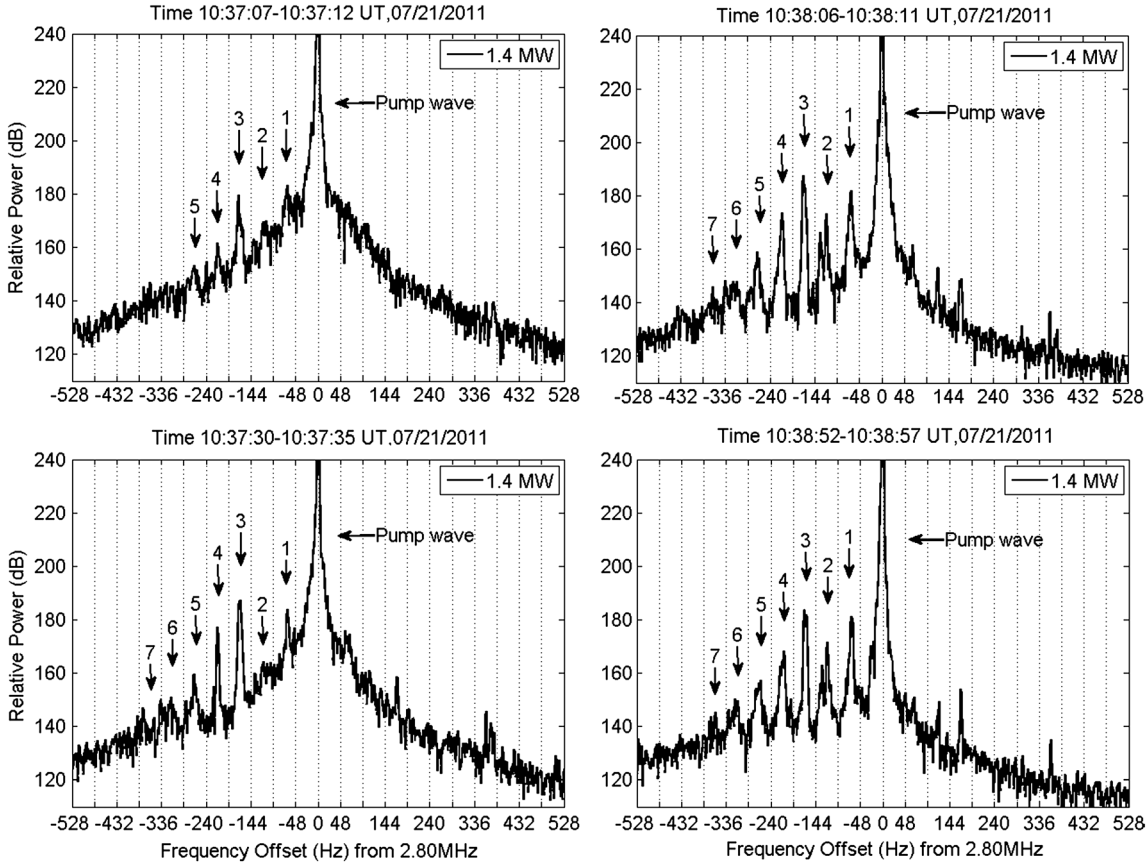

Figure 2. Stimulated electromagnetic emission spectra taken over 5 s intervals during 120 s heating demonstrates temporal evolution of the ion gyroharmonic structures. Note that structures start to appear above the noise level approximately 6 s after the heater turn-on. Dotted lines are at the ion gyrofrequency. Note that the third, fourth, and fifth have the fastest growth initially, and all the ion gyroharmonic structures are downshifted relative to the pump frequency.

was turned on. Thus, it can be inferred that the pump field decays into different neutralized IB modes simultaneously. Note that the third, fourth, and fifth structures have the fastest growth rate respectively.

3.2. Broadband Spectral Features

[11] In addition to the discrete ion gyroharmonic structures, occasionally a broadband spectral feature was observed within 1 kHz of the pump frequency during the heating experiments near the second electron gyroharmonic frequency. This broadband spectral feature may be observed alone or with embedded discrete ion gyroharmonic structures. Figure 4 shows the broadband feature for the experiment in which the heater was transmitting only for 22 s at $f_{\text{heater}} = 2.85$ MHz on 23 July 2011. The broadband feature appeared in the power spectrum immediately after the heater turn-on. According to the digital ionosonde data, the reflection altitude was 160 km. This broadband feature peaks at –436.7 Hz downshifted from the pump frequency. Furthermore, an upshifted broadband sideband peaks at +432 Hz, but weaker than the downshifted one, is also distinguishable. A second broadband spectral feature, which peaks at ±797 Hz on both sides of the heater frequency, is also observed. Similarly, the downshifted sideband is stronger than the upshifted one. Figure 5 displays the first downshifted broadband spectral feature with embedded

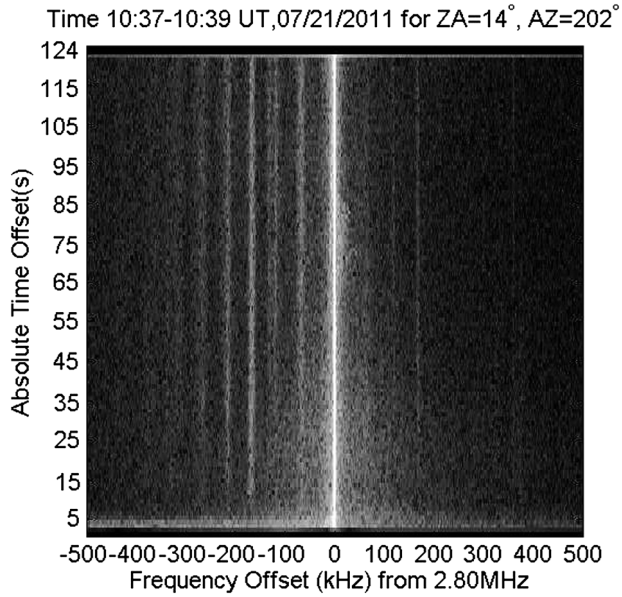

Figure 3. Spectrograph of the SEE structures in Figure 1. The strong line in the center with zero frequency offset is the pump wave and the discrete ion gyroharmonic structures are downshifted relative to the pump frequency.

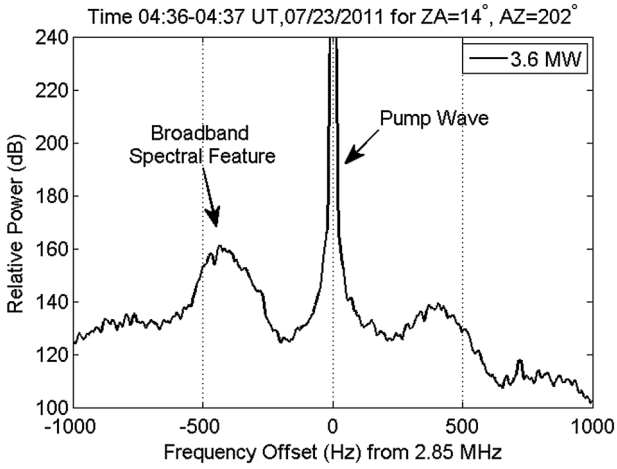

Figure 4. Experimental observation of the broadband spectral feature during which the heater frequency was 2.85 MHz and heating cycle was 22 s. Note that the broadband feature is downshifted relative to the pump frequency.

discrete structures corresponding to the 8th–10th harmonics of the ion gyrofrequency. The broadband feature peaks at –450 Hz relative to the pump frequency and seems to form right after the turn on. The second downshifted broadband feature is also recognizable. This experiment was conducted on 22 July 2011 in which the heater cycle was 30 s on at $f_{\text{heater}} = 2.77$ MHz. The reflection altitude was estimated to be 210 km. The ion gyrofrequency is estimated to be $f_{\text{ci}} = 48.9$ Hz. It should be noted that at the time of this experiment, the ionosphere was almost absent and the digital ionosonde does not give accurate estimation of the reflection altitude. In this experiment, the first upshifted broadband feature is very weak and the second one does not exist.

3.3. Possible Connection With Magnetized Stimulated Brillouin Scatter

[12] During the power stepping experiment conducted on 21 July 2011, in addition to the discrete ion gyroharmonic structures, another spectral line approximately 57 Hz downshifted relative to the pump field was observed for $P_{\text{heater}} \geq 1.8$ MW. This spectral line exhibits distinctly different features in comparison to the ion gyroharmonic structures. The threshold transmitter power that was required to generate this emission line was almost by a factor of two higher than the threshold level of the ion gyroharmonic structures. Its amplitude is noticeably larger. Its bandwidth is relatively narrower. It develops a few seconds later than other structures and its growth rate is faster. It usually damps out after a few tens of seconds. Figure 6 shows the high resolution power spectrum for $P_{\text{heater}} = 1.8$ MW (143 MW ERP), $P_{\text{heater}} = 1.4$ MW (111 MW ERP), and $P_{\text{heater}} = 0.4$ MW (31 MW ERP). Note only the ion gyroharmonic structure of the previous figures is observed for $P_{\text{heater}} = 1.4$ MW. Both spectral features can be seen for $P_{\text{heater}} = 1.8$ MW. The frequency resolution of the power spectrum was increased to 0.48 Hz (i.e., Fourier transform was taken over a longer period of time) to distinguish the first two spectral lines. Furthermore, the power spectrums were taken over a time interval from a few seconds after the transmitter turn-on to a few seconds before the turn-off. The heater duty cycle was 120 s on and 120 s off. The power spectrums of the SEE for transmission powers higher than $P_{\text{heater}} = 1.8$ MW are similar indicating that the threshold for both spectral features has been exceeded. Figure 7 is the spectrogram of the SEE acquired for $P_{\text{heater}} = 2.33$ MW (229 MW ERP). It is one of the best examples that clearly demonstrates growth and decay of the narrow spectral line near f_{ci}. This emission line is 57 Hz downshifted relative to the pump. The stronger amplitude of this spectral line relative to all the other ion gyroharmonic structures may imply direct involvement of the EM pump wave in the MSBS process. In other words, the pump EM wave directly decays to an ES low frequency decay mode and a backscattered EM wave. By comparing the acquired power spectrums with the previous experimental observations of the MSBS emission lines [*Bernhardt et al*., 2010], it may be inferred that the low frequency decay mode is electrostatic ion cyclotron (EIC) wave. Further comments will be made on this shortly.

[13] Figure 7 also shows that the second broader spectral line, very close to the first one, appears in the spectrogram earlier after the transmitter turn-on. This second spectral line with approximately 67 Hz frequency shift relative to the pump frequency is of course the first of the ion gyroharmonic structures as in the previous data figures.

4. Electric Field in the Interaction Region

[14] The generation mechanism of the ion gyroharmonic structures is proposed as a three-step process. First the EM pump field is converted to an ES UH/EB wave. A thermal OTSI that may be followed by the resonance instability is known as the conversion mechanism that creates field aligned irregularities (FAIs) in the interaction region [*Grach et al*., 1978; *Das and Fejer*, 1979; *Dysthe et al*., 1983; *Huang and Kuo*, 1994; *Inhester*, 1982; *Dysthe et al*., 1982; V*askov and Gurevich*, 1977]. In the next step, as will be discussed in the next section, the ES UH/EB wave decays into another ES UH/EB mode and several neutralized IB modes or an oblique IA wave. In the last step, the new generated

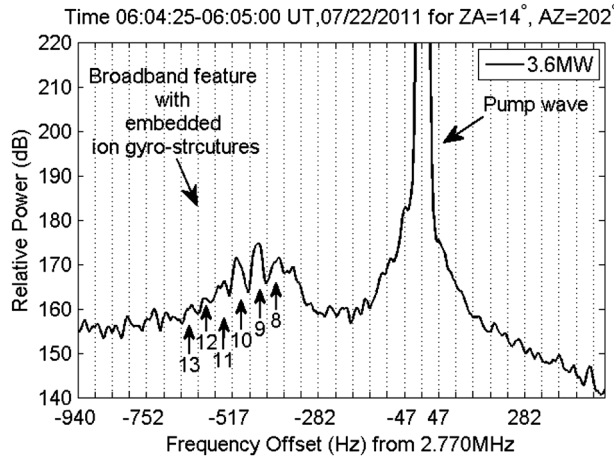

Figure 5. Experimental observations of broadband feature with embedded ion gyroharmonic structures during which the heater frequency was 2.77 MHz and heating cycle was 30 s. Dotted lines are at the ion gyrofrequency. Note that the spectral features are downshifted relative to the pump frequency.

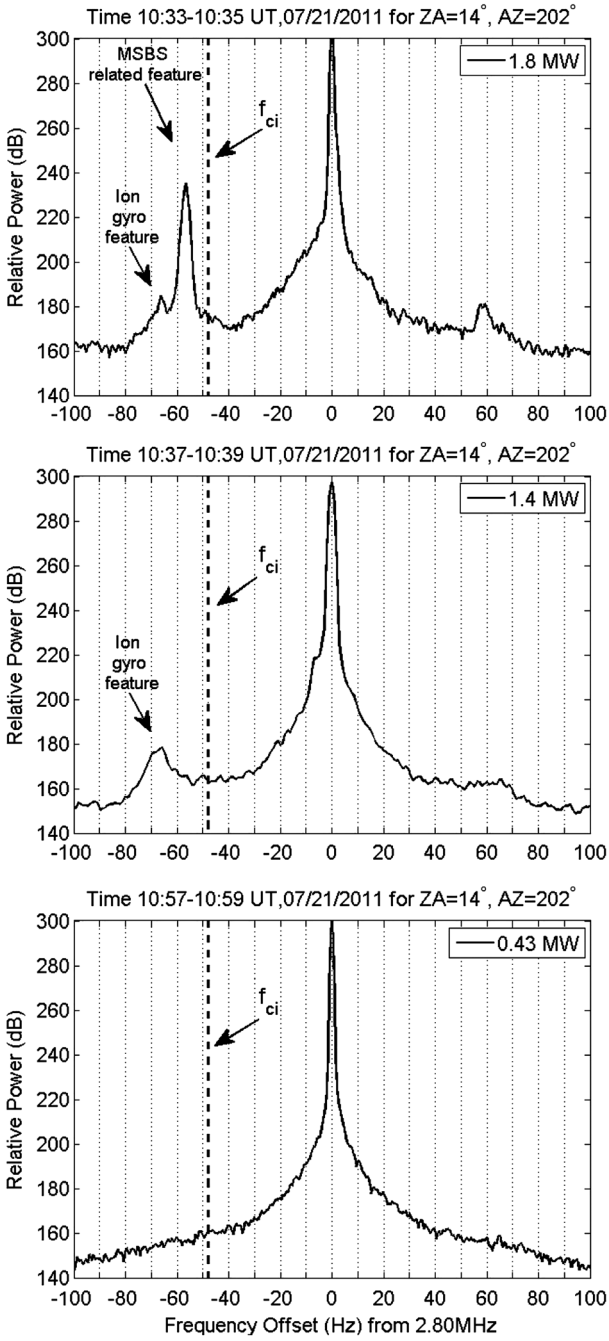

Figure 6. Possible experimental observation of the EIC emission line, downshifted relative to the pump frequency, generated through MSBS and the first mode of the discrete ion gyroharmonic structures shown in Figure 1. The heater frequency was 2.8 MHz and transmitter beam points to the magnetic zenith. Note that threshold level of the narrow emission line is near 1.8 MW, which is by a factor of two higher than the threshold level of the ion gyroharmonic structures (near 0.8 MW).

ES UH/EB mode, which exhibits frequency shift equal to the frequency of the neutralized IB or oblique IA decay modes (matching condition) is back converted to the EM wave. It is important to estimate the electric field strength in the interaction region (upper hybrid altitude) to access the viability of generation of the OTSI. In the ionosphere the refractive index is a function of height. Thus, the ionosphere is modeled as a horizontally stratified medium. By considering cold plasma approximation and using fluid equations in which the electrons are moving and ions are motionless background particles, the refractive index is approximated by

$$n^2_{\mathrm{O/X}} = 1 - \frac{X}{2D}\left\{2(1+iZ)(1+iZ-X) - Y^2\sin^2\theta \mp \left[Y^4\sin^4\theta + 4(1+iZ-X)^2Y^2\cos^2\theta\right]^{1/2}\right\} \quad (1)$$

where O and X in the subscript represent ordinary and extraordinary modes, $X = \omega^2_{\mathrm{pe}}/\omega^2$, $Y = \Omega_{\mathrm{ce}}/\omega$, $Z = \nu/\omega$, ν is the electron neutral collision frequency, ω_{pe} is the electron plasma angular frequency, Ω_{ce} is the electron cyclotron angular frequency, ω is the wave angular frequency and θ is the magnetic dip angle. D is defined as

$$D = [1+iZ-X]\left\{[1+iZ]^2 - Y^2\right\} - XY^2\sin^2\theta \quad (2)$$

[15] Exact EM wave equations in the ionosphere were derived by *Förstrling* [1942]. It is shown that in the slow varying medium, Förstrling equations for the ordinary mode can be simplified into [*Budden*, 1966]

$$\frac{\partial F_O}{\partial z} + k^2 n^2_O F_O = 0 \quad (3)$$

[16] The electric field in the ionosphere is given by

$$E_O = (\rho_X, 1, \rho_X\rho_{\mathrm{L,O}})F_O/\sqrt{\rho^2_X - 1} \quad (4)$$

where

$$\rho_{\mathrm{O/X}} = \frac{i}{2(1+iZ-X)Y\cos\theta}\left\{Y^2\sin^2\theta \pm \left[Y^4\sin^4\theta + 4(1+iZ-X)^2Y^2\cos^2\theta\right]^{1/2}\right\} \quad (5)$$

and

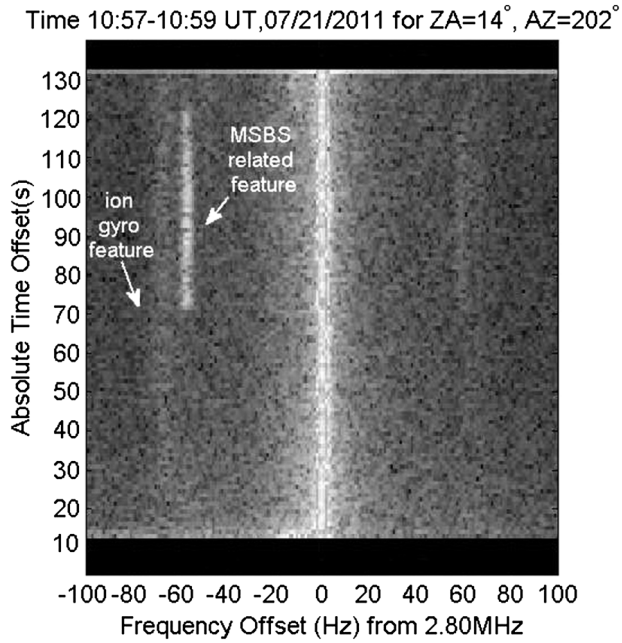

Figure 7. The spectrogram of the SEE for $\boldsymbol{P_{\mathrm{heater}}}$ = **2.33** MW. It clearly shows that the first spectral line develops late and damps out around 15 s before the heater turn-off. Its bandwidth is narrower than other structures.

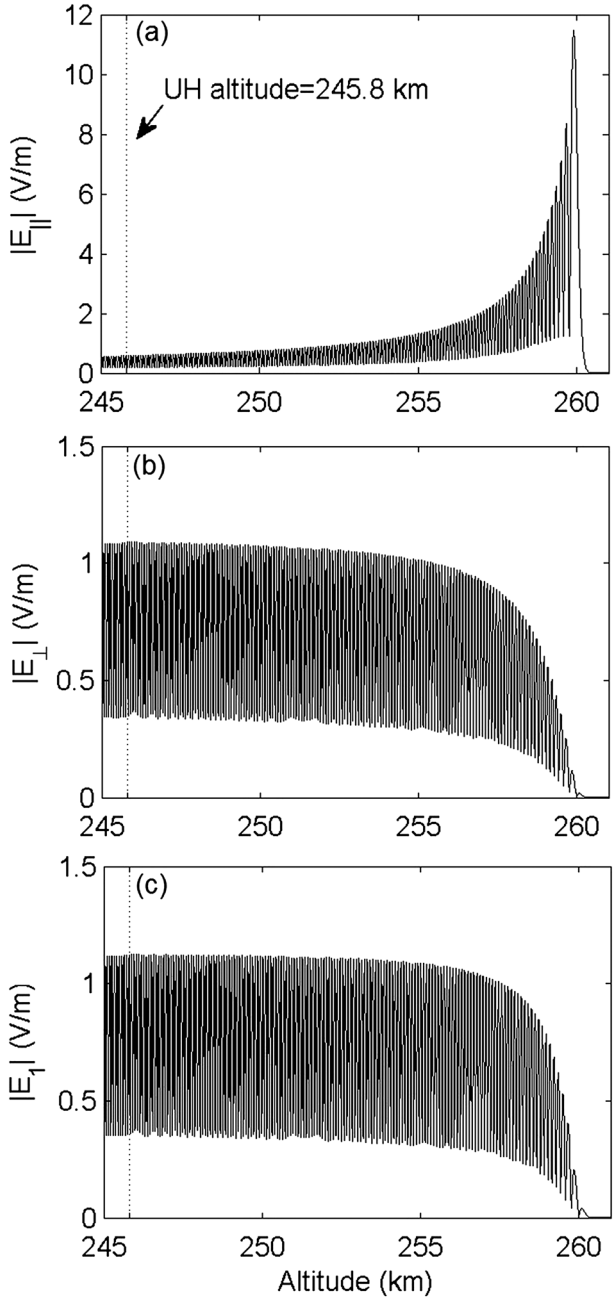

Figure 8. The electric field amplitude (a) along the magnetic field, $\boldsymbol{E}_{\parallel}$, (b) perpendicular to the magnetic field, $\boldsymbol{E}_{\perp}$, and (c) the east-west component $\boldsymbol{E}_{\mathbf{1}}$. The transmission frequency is 2.8 MHz and the magnetic dip angle is assumed to be 14°. The bottom of the ionosphere (reference point) is assumed to be at $z = 200$ km in which the electric field intensity 1 V/m is considered.

$$\rho_{\mathrm{L,O}} = \frac{iY\sin\theta}{1 + iZ - X}\left(n_O^2 - 1\right). \tag{6}$$

[17] All these equations can be found in *Lundborg and Thidé* [1985, 1986]. Far from the reflection altitude, the WKB method can be used to calculate the electric field with an acceptable approximation. However, close to the reflection altitude, the uniform approximation method provides a more precise solution to the wave equation. Details of this method can be found in the two consecutive papers by *Lundborg and Thidé* [1985, 1986]. We employed the uniform approximation method to estimate the electric field strength and its direction in between the upper hybrid and the reflection altitude. Because the heater frequency is far below the critical frequency, the monotonically increasing electron density model is used. The digital ionosonde data are used to approximate the electron density profile. Figure 8 displays the electric field components in between the upper hybrid altitude (z = 245.8 km) and the reflection altitude (z = 260 km). The electric field intensity at the reference point is 1 V/m. The reference point was chosen at z = 200 km using the digital ionosonde estimation of the F layer profile. According to this calculation, the relative intensity of the perpendicular electric field in the upper hybrid altitude is 1.08 V/m and the parallel component is 0.58 V/m, thus, the electric field is slightly off-perpendicular to the geomagnetic field in the upper hybrid altitude. The relative intensity of the total electric field in the upper hybrid altitude is $|E_{\mathrm{UH}}|/|E_{z=200\mathrm{km}}|$ = 1.67 V/m. On the other hand, slightly below the reflection altitude, at z = 259.9 km, the intensity of the perpendicular electric field is 0.08 V/m and the parallel component is 11.47 V/m; therefore, the electric field is parallel to the geomagnetic field. If we assume that the bottom of the ionosphere is at the reference point, which is z = 200 km, the electric field intensity in the upper hybrid altitude is $|E| = 1.67\sqrt{\eta_0 PG/4\pi z^2}$ where η_0 = 377 Ω is the impedance of free space, P is the heater power, and G = 19 dB is the antenna gain [*Bernhardt et al*., 2011]. The electric field intensity at the upper hybrid altitude corresponding to P_{heater} = 0.8 MW and P_{heater} = 3.6 MW are $|E|$ = 0.36 V/m and $|E|$ = 0.77 V/m, respectively. The next question is if this electric field intensity is strong enough to excite the OTSI. Previous studies of the OTSI shows that the threshold level could be as low as $|E|$ = 0.1 V/m [*Huang and Kuo*, 1995]. Past theoretical investigations of the threshold electric field intensity required to excite the OTSI have focused on the frequencies near the $n\Omega_{\mathrm{ce}}$ for $n \geq 3$. However, there are experimental evidences that for second electron gyroharmonic heating, FAIs are stronger than for higher gyroharmonics [*Fialer*, 1974; *Djuth et al*., 2005; *Kosch et al*., 2007; *Hysell and Nossa*, 2009]. Because FAIs are generated by the OTSI, it implies that the threshold electric field intensity may be even lower than $|E|$ = 0.1 V/m near 2 Ω_{ce}. Note that excitation of the thermal oscillating two-stream instability affects the electric field intensity above the upper hybrid altitude. This effect is not considered in the current calculations. Furthermore, the attenuation of the EM wave in the D region is also neglected in the calculations.

5. Theory and Results

[18] Parametric decay of the UH/EB pump wave into another UH/EB and neutralized IB wave has been introduced as a viable process for the generation of the ion gyroharmonic structures [*Scales et al*., 2011]. The neutralized ion Bernstein wave propagates slightly off-perpendicular to the background magnetic field exhibiting Boltzmann (neutralizing) electron behavior along the magnetic field and has different dispersive properties to the pure Bernstein mode, which propagates exactly perpendicular to the magnetic field [*Chen*,

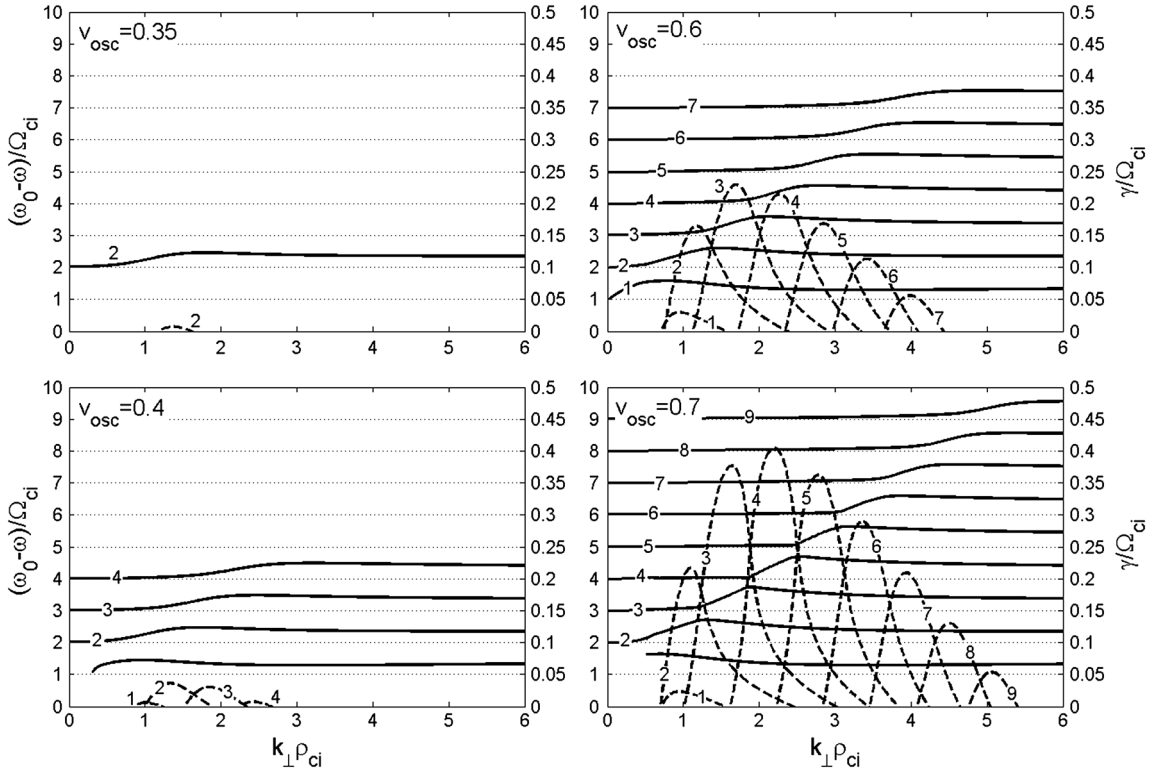

Figure 9. Dispersion relation of the low frequency decay mode (solid lines) and corresponding parametric decay instability growth rate (dashed lines) for $\boldsymbol{\theta_E = 4^\circ}$, $\boldsymbol{\omega_0 = 2\Omega_{ce} - 10\Omega_{ci}}$, $\boldsymbol{\nu_i = 3}$ Hz, $\boldsymbol{\nu_e = 400}$ Hz: (a) $\boldsymbol{v_{osc}/v_{te} = 0.35}$, (b) $\boldsymbol{v_{osc}/v_{te} = 0.4}$, (c) $\boldsymbol{v_{osc}/v_{te} = 0.6}$, and (d) $\boldsymbol{v_{osc}/v_{te} = 0.7}$ obtained from equation (7). Note that as the pump strength increases more harmonics are destabilized.

1984]. The other low frequency decay mode may also be an oblique IA wave for the broadband spectral feature. It should be noted that the neutralized IB and IA modes are intimately related in the sense that the mode surfaces are connected at oblique angles (e.g., *Kindel and Kennel* [1971] and *André* [1985]). This fact is critical in the interpretation of some of the SEE spectral structures. By enforcing wave number and frequency matching conditions, i.e., $\vec{k}_0 = \vec{k}_1 + \vec{k}_s$ and $\omega_0 = \omega_1 + \omega_s$, where subscripts 0, 1, and s represent parameters of the pump field, the high frequency decay mode, and the low frequency decay mode respectively, the general dispersion relation describing weak coupling is [*Porkolab*, 1974]

$$\varepsilon(\omega_s) + \frac{\beta_e^2}{4}\chi_i(\omega_s)\left\{\frac{\varepsilon_e(\omega_s)}{\varepsilon_e\left(-\omega_1^*\right)} - 2\right\} = 0 \tag{7}$$

where $\varepsilon(\omega) = 1 + \chi_e(\omega) + \chi_i(\omega)$, and $\varepsilon_e(\omega) = 1 + \chi_e(\omega)$. The susceptibility of the jth species is given by

$$\chi_j(\omega) = \frac{1}{k^2\lambda_{Dj}^2}\left\{\frac{1 + \zeta_{j0}\sum_{n=-\infty}^{\infty}\Gamma_n(b_j)Z(\zeta_{jn})}{1 + \frac{iv_j}{k_\parallel v_{tj}}\sum_{n=-\infty}^{\infty}\Gamma_n(b_j)Z(\zeta_{jn})}\right\} \tag{8}$$

where $b_j = k_\perp^2\rho_j^2$, k is the wave number, $k_\perp$ ($k_\parallel$) is the component of k perpendicular (parallel) to the magnetic field B, ρ_j is the gyroradius, $\zeta_{jn} = (\omega + iv_j - n\Omega_n)/k_\parallel v_{tj}$, Ω_n is the gyrofrequency, v_{tj} is the thermal velocity, v_j is the collision frequency, $\Gamma_n(b_j) = I_n(b_j)\exp(-b_j)$, Z is the Fried Conte function, I_n is the modified Bessel function of the first kind of order n, λ_{Dj} is the Debye length and β_e the coupling coefficient, proportional to the pump field E_0, is given by

$$\beta_e = \frac{e}{m_e}\left\{\left(\frac{E_{0\parallel}k_\parallel}{\omega_0^2} + \frac{E_{0x}k_x + E_{0y}k_y}{\omega_0^2 - \Omega_{ce}^2}\right)^2 + \frac{\left(E_{0x}k_y - E_{0y}k_x\right)^2\Omega_{ce}^2}{\omega_0^2\left(\omega_0^2 - \Omega_{ce}^2\right)^2}\right\}^{1/2} \tag{9}$$

and $k_\perp^2 = k_x^2 + k_y^2$.

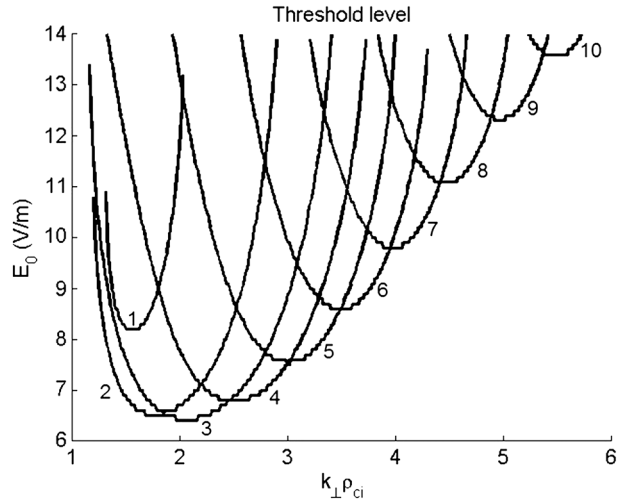

Figure 10. Threshold electric field intensity required for generation of each harmonic for $\boldsymbol{\theta_E = 4^\circ}$, $\boldsymbol{\omega_0 = 2\Omega_{ce} - 25\Omega_{ci}}$, $\boldsymbol{\nu_i = 1}$ **Hz** and $\boldsymbol{\nu_e = 400}$ Hz obtained from equation (7).

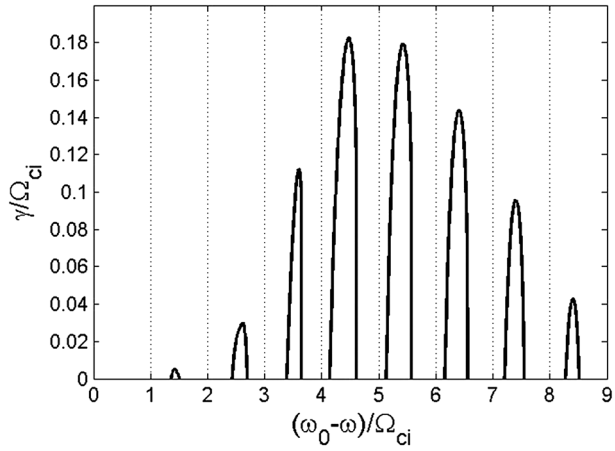

Figure 11. Growth rate versus frequency of the destabilized modes for $\boldsymbol{\theta_E = 4^\circ}$, $\boldsymbol{\omega_0 = 2\Omega_{ce} - 25\Omega_{ci}}$, $\boldsymbol{\nu_i = 1}$ Hz, $\boldsymbol{\nu_e =}$ **400 Hz** and $\boldsymbol{v_{osc}/v_{te} = 0.6}$ ($\boldsymbol{|E_0| = 12}$ **V/m**) obtained from equation (7).

[19] The pump wave is modeled using the dipole approximation, i.e., $k_0 = 0$. It should be noted that a more refined approach would be to assume the pump wave number is that of the field aligned irregularities generated from the OTSI [*Huang and Kuo*, 1995]. The simplified theory provided here will be shown to be adequate for initial interpretation of the experimental observations. A more refined framework will be the subject of future investigation.

[20] The Bernstein modes propagate almost perpendicular to the magnetic field; therefore, it is assumed that the parametric decay process occurs at the upper hybrid altitude in which, as was shown before, the electric field is almost perpendicular to the geomagnetic field; also, the double resonance condition is assumed for second gyroharmonic heating, i.e., $\omega_0 \approx \omega_{uh} = 2\Omega_{ce}$. The full dispersion relation is solved numerically for various parameter regimes. In all the calculations oxygen ions are assumed, the electron to ion temperature ratio $T_e/T_i = 3$, the ion-neutral collision frequency $\nu_i = 3$ Hz and the electron-neutral collision frequency $\nu_e = 400$ Hz except where noted. The electric field is assumed to be slightly off-perpendicular to the background magnetic field and the off-perpendicular angle is denoted by θ_E. The pump field strength is described by the electron oscillating velocity $v_{osc} = eE_0/m_e\omega_0$ where e is the electron charge. With no pump field, $v_{osc} = 0$, the solution of (7) will yield the normal modes. It is instructive to note the frequency shift of the spectral features from the pump frequency is essentially determined by the low-frequency decay modes. To reiterate, there are two primary low-frequency decay modes in this case. The first is the neutralized ion Bernstein mode otherwise known as the electrostatic ion cyclotron harmonic wave

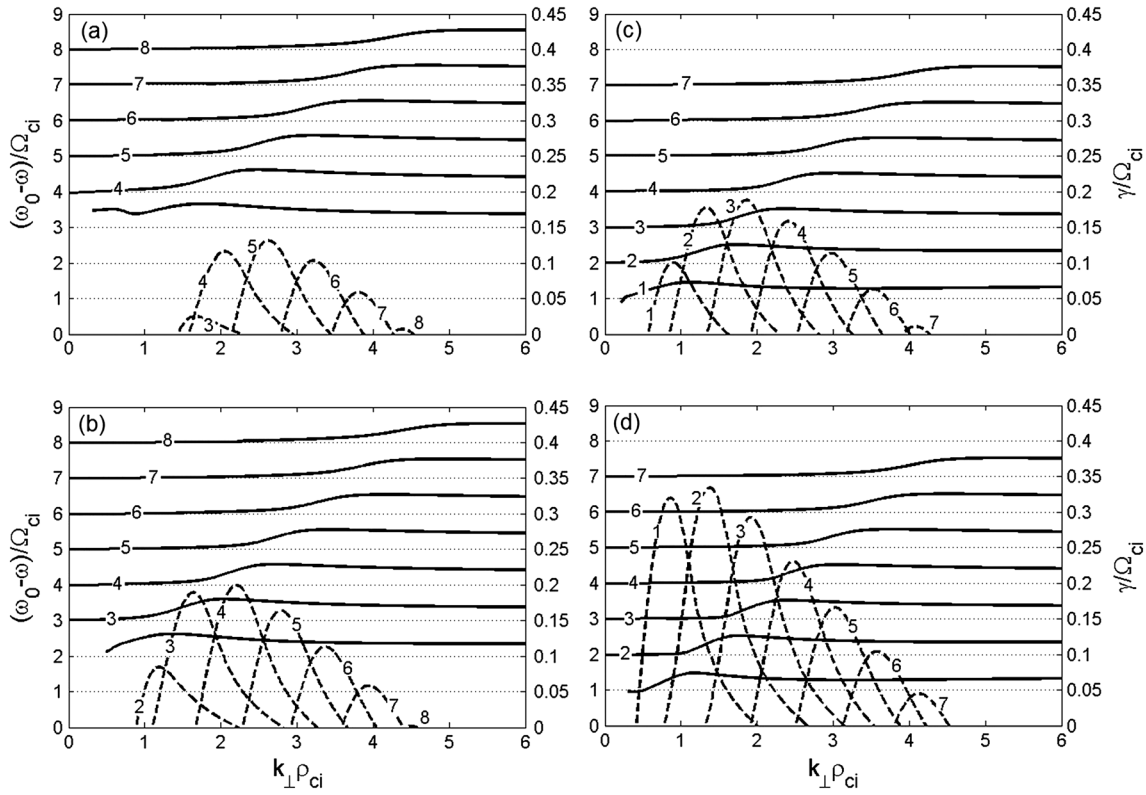

Figure 12. Dispersion relation for the low frequency decay mode (solid lines) and corresponding parametric decay instability growth rate (dashed lines) for $\boldsymbol{\theta_E = 4^\circ}$, $\boldsymbol{v_{osc}/v_{te} = 0.6}$, $\boldsymbol{\nu_i = 3}$ Hz, $\boldsymbol{\nu_e = 400}$ Hz: (a) $\boldsymbol{\omega_0 = 2\Omega_{ce} - 30\Omega_{ci}}$, (b) $\boldsymbol{\omega_0 = 2\Omega_{ce} - 15\Omega_{ci}}$, (c) $\boldsymbol{\omega_0 = 2\Omega_{ce} - \Omega_{ci}}$, and (d) $\boldsymbol{\omega_0 = 2\Omega_{ce} + 5\Omega_{ci}}$ obtained from equation (7). Note that increase of the offset frequency below $\boldsymbol{2\Omega_{ce}}$ moves the most excited harmonic to the higher modes.

(e.g., *Kindel and Kennel* [1971]). These have the dispersion relation

$$\omega \approx n\Omega_{ci}\left[1+\frac{T_e}{T_i}\Gamma_n\left(k_\perp^2\rho_i^2\right)\right] \tag{10}$$

for the nth harmonic. The perpendicular wavelength is determined roughly from $k_\perp\rho_{ci}\sim n$ and the parallel wavelength from $k_{||}/k_\perp\sim 0.1$. It is noted that the frequency shift above the gyroharmonic is determined by the ratio of T_e/T_i. The oblique IA wave is the other low frequency decay mode and has the dispersion relation approximated by

$$\omega \approx k_\perp c_s \tag{11}$$

where $c_s=\sqrt{KT_e/m_i}$ is the sound speed and K is Boltzmann constant. Figure 9 demonstrates the influence of the electron oscillating velocity on the ion gyroharmonic structures for $\theta_E = 4^\circ$ and $\omega_0=2\Omega_{ce}-10\Omega_{ci}$. It shows the dispersion relation of the low frequency decay mode (shift of the destabilized wave from the pump frequency) and the corresponding growth rate (i.e., $\omega_s=\omega+j\gamma$). Of course in this case, the dispersion relation is that of the neutralized ion Bernstein modes otherwise known as electrostatic ion cyclotron harmonic waves as stated earlier. The left vertical axis is normalized frequency (solid curves); the right is normalized growth rate (dashed curves), and the horizontal axis is the perpendicular normalized wave number. As the electric field strength increases, the number of destabilized modes also increases; the most excited mode changes from the second mode to the fourth mode. For this parameter regime, the second mode has the lowest threshold level. A more comprehensive study of the threshold level for $\nu_i=1$ Hz, $\nu_e=400$ Hz, $\omega_0=2\pi(2.8\times10^6)$ rad/s, $\theta_E=4^\circ$ and $\omega_0=2\Omega_{ce}-25\Omega_{ci}$ is shown in Figure 10. The third mode has the lowest threshold level. According to these calculations, the threshold electric field intensity for generation of 14 ion gyroharmonic structures by consideration of the damping rates is as low as 14 V/m. This electric field intensity is approximately by a factor of 20 less than the threshold level that was estimated for generation of ion gyroharmonic structures in the reflection altitude [*Bernhardt et al.*, 2011]. It is determined that for the higher ion-neutral collision frequencies, e.g., $\nu_i\sim 3$ Hz, the first and second modes are stable. The corresponding growth rate for $v_{osc}/v_{te}=0.6$ ($|E_0|=12$ V/m) is displayed versus frequency in Figure 11. For these parameters, maximum growth occurs in relatively narrow frequency bands with downshifts approximately at $(n+(1/2))\Omega_{ci}$ where n represents harmonic number. Although the third and second harmonics have the lowest threshold levels respectively, the fourth and fifth harmonics have higher growth rates if the pump field exceeds threshold. Figure 12 considers the effect of the pump offset frequency relative to the second electron gyroharmonic frequency on the destabilized modes, for $v_{osc}/v_{te}=0.6$ and $\theta_E=4^\circ$. Below the second electron gyroharmonic frequency, as the offset frequency of the pump field increases, the most excited mode shifts toward the higher modes. Furthermore, as the frequency offset increases, the lower harmonics (first, second, etc.) become stable (unless the ion-neutral collision frequency is somewhat lower). Whereas, above the second electron gyroharmonic frequency, the most excited mode is either the first or the second mode. The maximum growth rate was obtained when the pump frequency was slightly above the second electron gyroharmonic frequency $\omega_0\approx 2\Omega_{ce}+20\Omega_{ci}$. As the offset frequency relative to $\omega_0\approx 2\Omega_{ce}+20\Omega_{ci}$ increases, growth rate amplitude decreases so that at around $\pm 90\Omega_{ci}$ offset, all the decay modes are stable and the parametric decay instability does not occur. It should also be mentioned that for higher θ_E and lower ion-neutral and electron-neutral collision frequencies, at bigger offset frequencies such as $\pm 120\Omega_{ci}$, still a few of the modes can be destabilized.

[21] However, the angle of the pump field and collisional effects does not make a big difference in the maximum allowed offset frequency. The effect of θ_E on the low frequency decay mode is demonstrated in Figure 13 for $v_{osc}/v_{te}=0.5$ and $\omega_0=2\Omega_{ce}-20\Omega_{ci}$.

[22] As θ_E increases, the number of the destabilized harmonics also increases. Moreover, at higher θ_E, highly oblique IA waves with dispersion relation $\omega\approx k_\perp c_s$ is destabilized instead of discrete neutralized IB modes. The growth rate is almost by a factor of two higher. By comparing experimental observations and results of the growth rate calculations, it can be concluded that the broadband spectral feature most likely involves this decay mode. The simultaneous occurrence of the broadband spectral feature and the discrete ion gyroharmonic structure corresponds to the transition of the low frequency decay mode from the neutralized IB modes to oblique IA mode, which exhibits growth in a broad frequency band (Figure 13 for $\theta_E=7^\circ$). Figure 14 shows growth rate versus frequency, which is to some extent similar to the power spectrums obtained from the experimental measurements (see Figures 4 and 5). The parameter regime that is used in these calculations are exactly the same as Figures 13c and 13d. The top panel (Figure 14a) clearly displays the discrete ion gyroharmonic structures embedded in the broadband feature for $\theta_E=7^\circ$. The bottom panel (Figure 14b) shows the broadband spectral feature obtained for $\theta_E=8^\circ$. Note, if v_{osc} is reduced, e.g., $v_{osc}/v_{te}=0.4$, again, instead of the broadband feature, discrete ion gyroharmonics will be excited as in Figure 11. This indicates that the threshold electric field intensity that is required to excite discrete ion gyroharmonic structures is lower than that for the broadband spectral feature effectively. It should be noted that the broadband structures tend to develop when $\gamma/\Omega_{ci}\sim 1$ because the ions are unmagnetized.

6. Discussion and Conclusions

[23] In this study, new experimental observations of the discrete ion gyroharmonic structures and the broadband spectral features excited during heating around the second electron gyroharmonic frequency is presented. It is shown that the discrete ion gyroharmonic structures can be generated using low heater powers such as 0.8 MW (63 MW ERP). The broadband feature appears in the power spectrum almost immediately after the heater turn-on, which implies its faster growth in comparison to the discrete structures. It is also shown that during high power heating, i.e., $P_{heater}\geq$ 1.8 MW (143 MW ERP), in addition to the discrete ion gyroharmonic structures, another spectral line approximately 57 Hz downshifted from the pump appears in the spectrum. Different spectral features of this mode relative to the other structures, such as the threshold excitation transmission

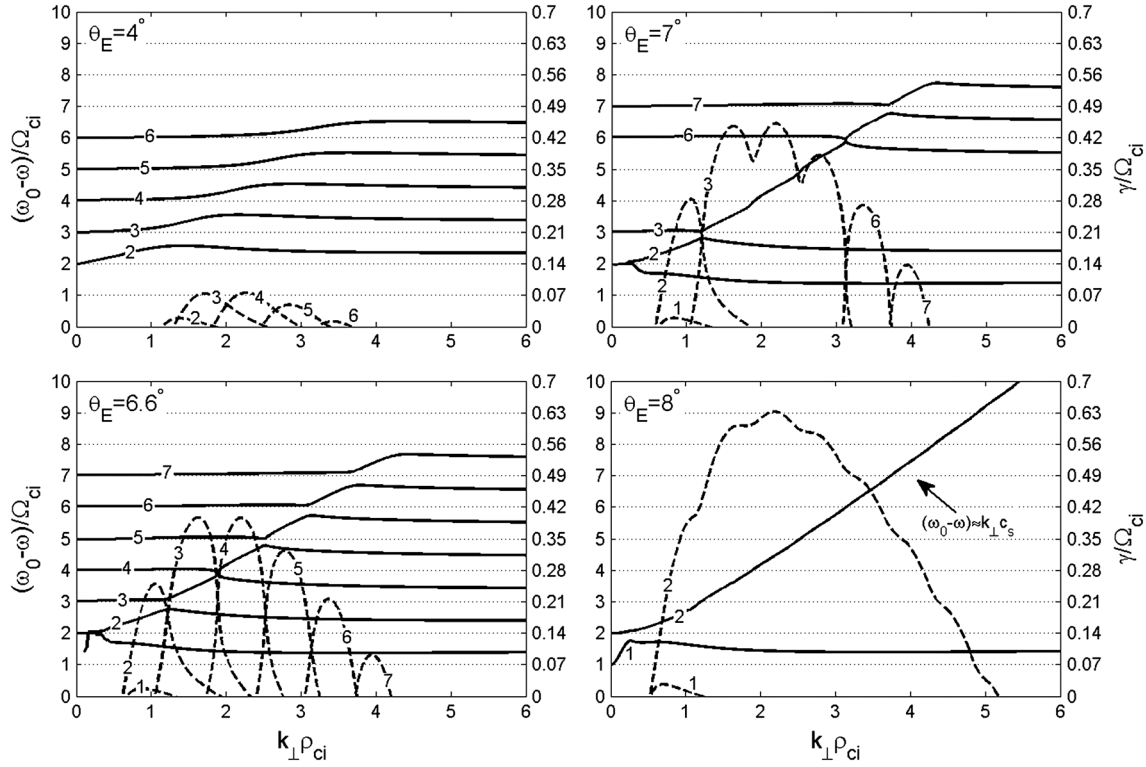

Figure 13. Dispersion relation for the low frequency decay mode (solid lines) and corresponding parametric decay instability growth rate (dashed lines) for $\boldsymbol{\omega_0 = 2\Omega_{ce} - 20\Omega_{ci}}$, $\boldsymbol{\nu_i = 3}$ Hz, $\boldsymbol{\nu_e = 400}$ Hz, $\boldsymbol{v_{osc}/v_{te} = 0.5}$: (a) $\boldsymbol{\theta_E = 4^\circ}$, (b) $\boldsymbol{\theta_E = 6.6^\circ}$, (c) $\boldsymbol{\theta_E = 7^\circ}$, and (d) $\boldsymbol{\theta_E = 8^\circ}$ obtained from equation (7) that demonstrates transition of the low frequency decay product from neutralized ion Bernstein to an oblique ion acoustic mode.

power, its strength, growth rate, bandwidth, frequency shift, damping, and development time, are indicative of another generation mechanism, possibly MSBS. The threshold transmission power for the generation of this spectral feature is 1.8 MW, which is by a factor of two higher than ion gyroharmonic structures. This emission line may be due to the parametric decay of the EM pump wave into an EIC wave and backscattered EM wave. This parametric decay process occurs in the longer wavelength regime, e.g., $k_\perp \rho_{ci} \ll 1$. Whereas, neutralized IB parametric decay waves have $k_\perp \rho_{ci} \geq 1$. In this case some of the characteristics could be explained. Note for longer wavelengths equation (10) reduces to

$$\omega \approx \Omega_{ci}\left(1 + \frac{k_\perp^2 c_s^2}{\Omega_{ci}^2}\right). \tag{12}$$

[24] This would explain the narrowness of the emission bandwidth and the smaller frequency shift, i.e., 57 Hz, observed in the data. Currently, no kinetic theory calculations exist for MSBS, which are required for this application and it is beyond the scope of the current work. A potential framework exists [*Stenflo*, 1999] and this is perhaps the subject of a future study.

[25] Parametric decay of the UH/EB pump field into another UH/EB and neutralized IB waves in the upper hybrid altitude is considered as a viable process for generation of the discrete ion gyroharmonic structures in the SEE spectrum. It is shown that the direction of the electric field component of the pump wave is changing from almost perpendicular to the geomagnetic field in the upper hybrid altitude to parallel to the geomagnetic field in the reflection altitude that is around 15 km above. It is consistent with the results of the previous studies [*Lundborg and Thidé*, 1986; *Leyser*, 1991; *Bernhardt et al*., 2009]. Because Bernstein waves are propagating almost perpendicular to the magnetic field, occurrence of the process in the upper hybrid altitude seems more reasonable than the reflection altitude. It is also shown that at $\theta_E \geq 7^\circ$, the UH/EB pump field decays into another UH/EB mode and a broadband oblique IA mode that is consistent with the generation mechanism of the broadband spectral feature. Although θ_E depends on the density of the ionosphere, it also should be roughly related to the transmitter beam angle. The digital ionosonde data corresponding to times when the broadband spectral feature is observed clearly shows that the ionospheric density is much higher than when the discrete structures were observed. The pump EM wave experiences more bending in the denser ionosphere, implying higher θ_E. The analytical model predicts that the growth rate of the oblique IA mode is by a factor of two larger than the neutralized IB modes. This prediction is in line with the experimental observation of the broadband feature growing faster than the discrete ion gyroharmonic spectral features.

[26] It is demonstrated that the threshold electric field intensity for the proposed mechanism is approximately,

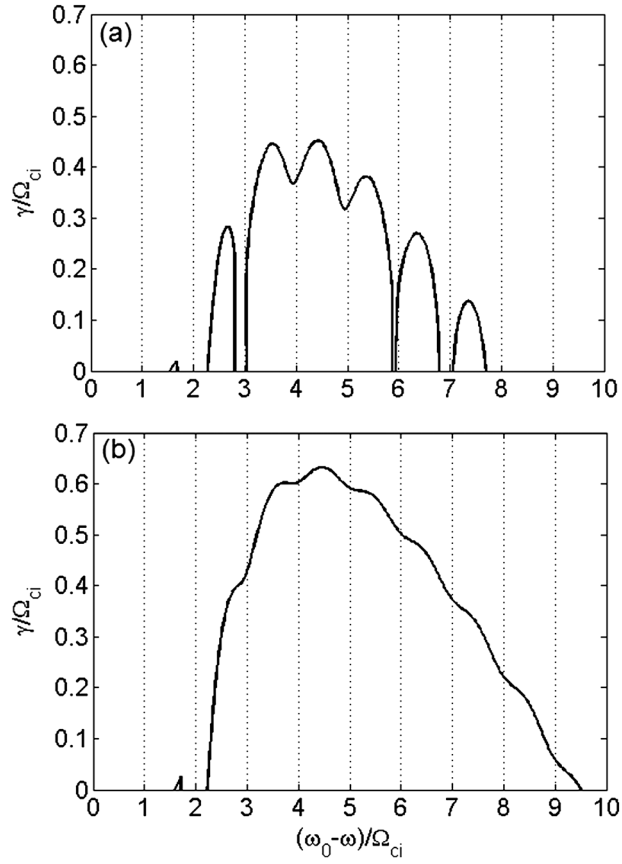

Figure 14. Growth rate versus frequency of the destabilized modes for $\omega_0 = 2\Omega_{ce} - 20\Omega_{ci}$, $\nu_i = 3$ Hz, $\nu_e = 400$ Hz, $\nu_{osc}/\nu_{te} = 0.5$: (a) $\theta_E = 7°$ and (b) $\theta_E = 8°$ obtained from equation (7). Note, as θ_E increases, first, the discrete ion gyroharmonic structures embed in the broadband feature and then just the broadband spectral feature is excited.

6 V/m, which is much less than 250 V/m that was predicted for the generation process in the reflection altitude [*Bernhardt et al*., 2011].

[27] It is observed that the maximum growth rate of the neutralized ion Bernstein modes occurs when the pump frequency is slightly above the second electron gyroharmonic frequency. Whenever the pump frequency is above the second electron gyroharmonic frequency, the first or second harmonic has the highest growth rate. Whereas, higher harmonics such as the third, fourth, and even up to the eighth mode, have the highest growth rates when the pump frequency is below the second electron gyroharmonic frequency and its offset frequency increases. Because in the experimental observations the third and the fourth modes have the fastest growth, it may be concluded that the transmitter frequency is below $2\Omega_{ce}$, which is in line with the digital ionosonde estimation of the electron gyrofrequency. A stronger pump field destabilizes more harmonics. It may also influence on the most excited mode, but the frequency of the pump field has the dominant effect. As the off-perpendicular angle θ_E of the pump field relative to the background magnetic field increases, the threshold pump field intensity reduces, the number of destabilized neutralized IB modes increases, and gradually an oblique IA wave mode is excited instead of neutralized IB modes. Finally, it is important to note that the theory predicts these structures are all excited most strongly in the interaction region where the pump frequency is within several kHz of $2\Omega_{ce}$. Such behavior has been observed in experiments where the pump frequency was swept through $2\Omega_{ce}$ [H. Fu, personal communication, 2012]. It should be noted that much of the same behavior described here is also observed at experiments near $3\Omega_{ce}$ [A. Mahmoudian et al., Ion gyro-harmonic structuring in the stimulated radiation spectrum and optical emissions during electron gyro-harmonic heating, submitted to *Journal of Geophysical Research*, 2012].

[28] As was mentioned before, the broadband spectral feature is most likely due to parametric decay into an IA wave that is excited at higher θ_E. It should be noted that the threshold electric field intensity for excitation of the oblique IA mode is higher than the neutralized IB modes, thus even at higher θ_E in the low power heating experiments, discrete ion gyroharmonic structures are expected to be observed. The observations reported in this paper were carried out at the HAARP facility. Another prominent SEE feature, the DP [*Leyser*, 2001], which has most thoroughly been investigated at the European Incoherent SCATer radar (EISCAT) facility for higher gyroharmonic heating ($n > 2$), has a number of similarities with the broadband spectral feature observed here. The DP has also been proposed as being due to parametric decay involving obliquely propagating ion acoustic waves [*Huang and Kuo*, 1995]. More careful studies, both experimental and theoretical calculations, are needed to determine the connection between these two spectral features especially considering the established importance of the DP behavior as a diagnostic for heating near electron gyroharmonics in general [*Tereshchenko et al*., 2006]. The broadband spectral feature observed here for second electron gyroharmonic heating may ultimately allow at least similar diagnostic information as the DP.

[29] Other possible nonlinear processes during the heating experiments can be studied using a more sophisticated particle-in-cell numerical model. Numerical simulation and corresponding considerations will be the subject of a companion paper. Generation mechanism of the second downshifted broadband feature and upshifted sidebands are beyond the scope of this research and will be the subject for future investigations. The prerequisite of the generation mechanism that is considered in this paper is conversion of the EM pump wave into the ES UH/EB pump wave. This mode conversion process generates FAI and anomalous absorption in the interaction region. In contrast to the heating near $n\Omega_{ce}$ for $n \geq 3$, for which FAIs are suppressed, there are experimental evidences that near the second electron gyroharmonic heating, FAIs are even stronger [*Fialer*, 1974; *Djuth et al*., 2005; *Kosch et al*., 2007; *Hysell and Nossa*, 2009]. These experimental evidences justify presumption of the proposed decay process. It should be the subject of future experiments to determine if FAIs, anomalous absorption, and airglow can be observed at the same time when the ion gyroharmonic structures are observed in the SEE spectrum.

[30] A number of unanswered questions still remain about the SEE spectral features discussed here and more experiments are warranted. At this time, the distinguishing observational characteristics of the discrete and broadband spectra

are ionospheric density gradient related as described in section 2. More systematic experiments, guided by the theoretical predictions here, are required to definitively determine the conditions for the transition from the discrete to broadband spectral features. Moreover, the development of the OTSI and more importantly the resonance instability can cause wave trapping, which results in the hysteresis behavior of the ionosphere called preconditioning [*Hysell and Nossa*, 2009; *Wright et al*., 2009]. The preconditioning effects on the threshold and evolution of the aforementioned SEE spectral features will be the subject of future experiments.

[31] **Acknowledgments.** This work was supported by the National Science Foundation.

References

André, M. (1985), Dispersion surfaces, *J. Plasma Phys.*, *33*, 1–19, doi:10.1017/S0022377800002270.

Bernhardt, P. A., L. S. Wagner, J. A. Goldstein, V. Yu. Trakhtengerts, E. N. Ermakova, V. O. Rapoport, G. P. Komrakov, and A. M. Babichneko (1994), Enhancement of stimulated electromagnetic emission during two frequency ionospheric heating experiments, *Phys. Rev. Lett.*, *72*(18), 2879–2882, doi:10.1103/PhysRevLett.72.2879.

Bernhardt, P. A., C. A. Selcher, R.H. Lehmberg, J. Rodriguez, J. Thomason, M. McCarrick, and G. Frazer (2009), Determination of the electron temperature in the modified ionosphere over HAARP using the HF pumped stimulated Brillouin scatter (SBS) emmision lines, *Ann. Geophys.*, *27*, 4409–4427, doi:10.5194/angeo-27-4409-2009.

Bernhardt, P. A., C. A. Selcher, R. H. Lehmberg, S. P. Rodriguez, J. F. Thomason, K. M. Groves, M. J. McCarrick, and G. J. Frazer (2010), Stimulated Brillouin scatter in a magnetized ionospheric plasma, *Phys. Rev. Lett.*, *104*(16), 165004, doi:10.1103/PhysRevLett.104.165004.

Bernhardt, P. A., C. Selcher, and S. Kowtha (2011), Electron and ion Bernstein wave excited in the ionosphere by high power EM waves at the second harmonic of the electron cyclotron frequency, *Geophys. Res. Lett.*, *38*, L19107, doi:10.1029/2011GL049390.

Budden, K. G. (1966), *Radio Waves in the Ionosphere?*, Cambridge University Press, New York.

Chen, F. F. (1984), *Introduction to Plasma Physics and Controlled Fusion*, vol. 1, *Plasma Physics*, Springer, 2nd ed.

Das, A. C., and J. A. Fejer (1979), Resonance instability of small-scale field-aligned irregularities, *J. Geophys. Res.*, *84*(A11), 6701–6704, doi:10.1029/JA084iA11p06701.

Djuth, F. T., T. R. Pedersen, E. A. Gerken, P. A. Bernhardt, C. A. Selcher, W. A. Bristow, and M. J. Kosch (2005), Ionospheric modification at twice the electron cyclotron frequency, *Phys. Rev. Lett.*, *94*(12), 125001, doi:10.1103/PhysRevLett.94.125001.

Dysthe, K. B., E. Mjølhus, H. Pécseli and K. Rypdal (1982), Thermal cavitons, *Phys. Scr.*, *26*, 548, doi:10.1088/0031-8949/1982/T2B/040.

Dysthe, K. B., E. Mjølhus, H. L. Pécseli, and K. Rypdal (1983), A thermal oscillating two-stream instability, *Phys. Fluids*, *26*, 146, doi:http://dx.doi.org/10.1063/1.863993.

Fialer, P. A. (1974), Field-aligned scattering from a heated region of the ionosphere-observations at HF and VHF, *Radio Sci.*, *9*(11), 923–940, doi:10.1029/RS009i011p00923.

Förstrling, K. (1942), Über die Ausbreitung Elelctromagnetischer Wellen in einem Magnetisierten Medium bei Senkrechter Incidencz, *Hochfr. Elek. 59*, 10–22.

Grach, S. M., A. N. Karashtin, N. A. Mityzkov, V. O. Rapoport, and V. Y. Trakhtengerts (1978), Theory of thermal parametric instability in an inhomogenous plasma, *Sov. J. Plasma Phys., Engl. Transl. 4*, 4, 737–741.

Huang, J., and S. P. Kuo (1994), Cyclotron harmonic effect on the thermal oscillating two-stream instability in the high latitude ionosphere, *J. Geophys. Res.*, *99*(A2), 2173–2181, doi:10.1029/93JA02668.

Huang, J., and S. P. Kuo (1995), A generation mechanism for the downshifted peak in stimulated electromagnetic emission spectrum, *J. Geophys. Res. 100*(A11), 21,433–21,438, doi:10.1029/95JA02302.

Hysell, D. L., and E. Nossa (2009), Artificial E-region field-aligned plasma irregularities generated at pump frequencies near the second electron gyroharmonic, *Ann. Geophys.*, *27*, 2711–2720, doi:10.5194/angeo-27-2711-2009.

Inhester, B. (1982), Thermal modulation of the plasma density in ionospheric heating experiments, *J. Atmos. Terr.*, *44*(12), 21,1049–1059, doi:10.1016/0021-9169(82)90017-4.

Kindel, J. M., and C. F. Kennel (1971), Topside current instabilities, *J. Geophys. Res.*, *76*(13), 3055–3078, doi:10.1029/JA076i013p03055.

Kosch, M. J., T. Pedersen, E. Mishin, S. Oyama, J. Hughes, A. Senior, B. Watkins, and B. Bristow (2007), Coordinated optical and radar observations of ionospheric pumping for a frequency pass through the second electron gyroharmonic at HAARP, *J. Geophys. Res.*, *112*, A06325, doi:10.1029/2006JA012146.

Leyser, T. B. (1991), Parametric interaction between upper hybrid and lower hybrid waves in heating experiments, *Geophys. Res. Lett.*, *18*(3), 408–411, doi:10.1029/91GL00136.

Leyser, T. B., B. Thidé, S. Goodman, M. Waldenvik, E. Veszelei, S. M. Grach, A. N. Karashtin,G. P. Komrakov, and D. S. Kotik (1992), Narrow cyclotron harmonic absorption resonances of stimulated electromagnetic emission in the ionosphere, *Phys. Rev. Lett.*, *68*(22), 3299–3302, doi:10.1103/PhysRevLett.68.3299.

Leyser, T. B. (2001), Stimulated electromagnetic emission by high-frequency electromagnetic pumping of the ionospheric plasma, *Space Science Reviews*, *98*, 223–328, doi:10.1023/A:1013875603938.

Lundborg, B., and B. Thidé (1985), Standing wave pattern of HF radio waves in the ionospheric reflection region 1. General formulas, *Radio Sci.*, *20*(4), 947–957, doi:10.1029/RS020i004p00947.

Lundborg, B., and B. Thidé (1986), Standing wave pattern of HF radio waves in the ionospheric reflection region 2. Applications, *Radio Sci.*, *21*(3), 486–500, doi:10.1029/RS021i003p00486.

Norin, L., T. B. Leyser, E. Nordblad, B. Thidé, and M. McCarrick (2009), Unprecedentedly strong and narrow electromagnetic emissions stimulated by high-frequency radio waves in the ionosphere, *Phys. Rev. Lett.*, *102*(6), 065003, doi:10.1103/PhysRevLett.102.065003.

Pedersen, T., B. Gustavsson, E. Mishin, E. Kendall, T. Mills, H. C. Carlson, and A. L. Snyder (2010), Creation of artificial ionospheric layers using high-power HF waves, *Geophys. Res. Lett.*, *102*(37), L02106, doi:10.1029/2009GL041895.

Pedersen, T., M. McCarrick, B. Reinisch, B. Watkins, R. Hamel, and V. Paznukhov (2011), Production of artificial ionospheric layers by frequency sweeping near the 2nd gyroharmonic, *Ann. Geophys.*, *102*(29), 47–51, doi:10.5194/angeo-29-47-2011.

Porkolab, M. (1974), Theory of parametric instability near the lower-hybrid frequency, *Phys. Fluids*, *17*, 1432–1442, doi:10.1063/1.1694910.

Scales, W. A., M. R. Bordikar, A. Samimi, P. A. Bernhardt, S. Briczinski, C. A. Selcher, and M. McCarrick (2011), Observations and theory of ion gyro-harmonic structures in the stimulated radiation spectrum during second electron gyro-harmonic heating, *General Assembly and Scientific Symposium, URSI*, doi:10.1109/URSIGASS.2011.6051126.

Sharma, R. P., A. Kumar, and R. Kumar (1993), Excitation of ion-Bernstein waves in ionospheric modification experiment, *Radio Sci. 28*(6), 951–957, doi:10.1029/93RS01374.

Stenflo, L. (1999), Theory of stimulated scattering of large-amplitude waves, *J. Plasma Phys.*, *61*, pp. 129-134, doi: http://dx.doi.org/10.1017/S0022377800008655.

Tereshchenko, E. D., R. Yu. Yurik, B. Z. Khudukon, M. T. Rietveld, B. Isham, V. Belyey, A. Brekke, T. Hagfors, and M. Grill (2006), Directional features of the downshifted peak observed in HF-induced stimulated electromagnetic emission spectra obtained using an interferometer, *Ann. Geophys.*, *61*(24), 1819–1827, doi:10.5194/angeo-24-1819-2006.

Thidé, B., H. Kopka, and P. Stubbe (1982), Observation of stimulated scattering of a strong high frequency radio wave in the ionosphere, *Phys. Rev. Lett.*, *49*, 1561–1564, doi:10.1103/PhysRevLett.49.1561.

Thidé, B., H. Derblom, Å. Hedberg, H. Kopka, and P. Stubbe (1983), Observations of stimulated electromagnetic emissions in ionospheric heating experiments, *Radio Sci.*, *18*(6), 851–859, doi:10.1029/RS018i006p00851.

Vaskov, V. V., and A. V. Gurevich (1977), Resonance instability of small-scale plasma perturbations, *Sov. Phys. JETP Engl. Trans.*, *46*, 487.

Wright, D. M., R. S. Dhillon, T. K. Yeoman, T. R. Robinson, E. C. Thomas, L. J. Baddeley, and S. Imber (2009), Excitation thresholds of field-aligned irregularities and associated ionospheric hysteresis at very high latitudes observed using SPEAR-induced HF radar backscatter, *Ann. Geophys.*, *27*, 2623–2631, doi:10.5194/angeo-27-2623-2009.

Zhou, H. L., J. Huang, and S. P. Kuo (1994), Cascading of the upper hybrid/electron Bernstein wave in ionospheric heating experiments, *Phys. Plasmas*, *1*(9), 3044–3052, doi:http://dx.doi.org/10.1063/1.870929.